

See discussions, stats, and author profiles for this publication at: <https://www.researchgate.net/publication/241696121>

On the Importance of Unprecedented Lone Pair–Salt Bridge Interactions in Cu(II)–Malonate–2–Amino-5-Chloropyridine–Perchlorate Ternary System

ARTICLE *in* THE JOURNAL OF PHYSICAL CHEMISTRY A · JUNE 2013

Impact Factor: 2.69 · DOI: 10.1021/jp4046066 · Source: PubMed

CITATIONS

3

READS

59

9 AUTHORS, INCLUDING:



Saikat Kumar Seth

Mugberia Gangadhar Mahavidyalaya, West Be...

49 PUBLICATIONS 557 CITATIONS

[SEE PROFILE](#)



Antonio Bauza

University of the Balearic Islands

101 PUBLICATIONS 710 CITATIONS

[SEE PROFILE](#)



Somnath Ray Choudhury

Jadavpur University

30 PUBLICATIONS 518 CITATIONS

[SEE PROFILE](#)



Subrata Mukhopadhyay

Jadavpur University

90 PUBLICATIONS 1,254 CITATIONS

[SEE PROFILE](#)

On the Importance of Unprecedented Lone Pair–Salt Bridge Interactions in Cu(II)–Malonate–2-Amino-5-Chloropyridine–Perchlorate Ternary System

Monojit Mitra,[†] Prankrishna Manna,[†] Amrita Das,[†] Saikat Kumar Seth,[‡] Madeleine Helliwell,[§] Antonio Bauzá,^{||} Somnath Ray Choudhury,^{*,†} Antonio Frontera,^{*,||} and Subrata Mukhopadhyay^{*,†}

[†]Department of Chemistry, Jadavpur University, Kolkata 700 032, India

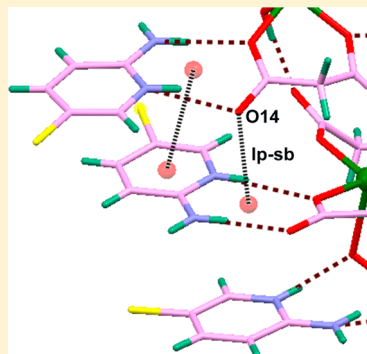
[‡]Department of Physics, M. G. Mahavidyalaya, Bhupatinagar, Midnapore (East), West Bengal 721 425, India

[§]School of Chemistry, The University of Manchester, Brunswick Street, Manchester, M13 9PL, United Kingdom

^{||}Departament de Química, Universitat de les Illes Balears, Crt. de Valldemossa km 7.5, 07122 Palma (Baleares), Spain

Supporting Information

ABSTRACT: A Cu(II)–malonate complex with formula $\{(C_5H_6N_2Cl)_12[Cu(1)(C_3H_2O_4)_2][Cu(2)(C_3H_2O_4)_2(H_2O_2)][Cu(4)(C_3H_2O_4)_2][Cu(3)(C_3H_2O_4)_2(H_2O_2)](ClO_4)_4\}$ (**1**) [$C_5H_6N_2Cl$ = protonated 2-amino-5-chloropyridine, $C_3H_2O_4$ = malonic acid, ClO_4^- = perchlorate] has been synthesized from purely aqueous media simple by mixing the reactants in their stoichiometric ratio, and its crystal structure has been determined by single-crystal X-ray diffraction. In **1**, copper(II) malonate units form infinite 1D polymeric chains, which are interlinked by hydrogen bonds to generate 2D sheets. These 2D sheets are joined side by side primarily by various hydrogen bonds to form a 3D structure. A multitude of salt bridges are formed in this structure, connecting the protonated 2-amino-5-chloropyridines and the malonate ligands of the polymeric polyanion. Examining this characteristic of the solid-state architecture, we noticed several salt-bridge (sb)– π interactions and an unexplored interaction between the lone pair (lp) of one malonate oxygen atom and a planar salt bridge. The combination of this interaction with various other weak intermolecular forces results in a remarkably extended supramolecular network combining a wide variety of interactions involving π –systems ($Cl\cdots\pi$, $\pi\cdots\pi$) and salt bridges (sb– π and lp–sb). We describe the energetic and geometric features of this lone pair–salt-bridge interaction and explore its impact on the resultant supramolecular organization using theoretical DFT-D3 calculations.



1. INTRODUCTION

Supramolecular chemistry relies on weak noncovalent interactions whose manifestation has been observed in all areas of chemistry, where supramolecular chemists and crystal engineers have controlled molecular organization by judicious manipulation of interactions between molecules. In this context, interactions involving aromatic systems are particularly important because they can exert enormous influence in chemical and biological processes when present en masse.^{1–6} Recently, two new types of supramolecular bonding forces, viz. the anion– π and lone-pair– π (lp– π) interactions, have attracted much attention from the scientific community worldwide for being potentially important from the supramolecular perspective.^{7,8} This initiated the study of the physical nature and quantification of these particular forces by means of theoretical and experimental investigations.⁹ In addition, stacking interactions between H-bonding arrays and aromatic rings have received little attention until now.¹⁰

Recently a favorable binding energy between a planar salt bridge (H-bonding array) forming a stacking complex with aromatic rings was described. The system was explored by

means of theoretical calculations, and moreover experimental support was obtained from the CSD.¹⁰ In addition, in the crystal lattice of a Cu(II) malonate complex the supramolecular network observed in the solid state is partially sustained by the formation of a salt-bridge– π (sb– π) interaction.¹⁰ Remarkably, because of the ion pair nature of the salt bridge, the interaction with an aromatic ring can be defined as cation– π , anion– π , or sb– π , depending on the position of the aromatic ring under the salt bridge. The sb– π interaction corresponds to the parallel stacking between the arene and the planar salt bridge, forming a sandwich (not displaced). Curiously, the interaction is favorable for both electron-rich and electron-poor arenes.

Although the formation of salt bridges is not favorable in aqueous solution due to strong solvation effects,¹¹ they are very important in protein chemistry.¹² This is due to the important and specific functions played by them as binding sites in enzymes mediating molecular recognition.¹³ They are also

Received: May 9, 2013

Revised: June 20, 2013

Published: June 24, 2013



involved in determining the stability of secondary-structural elements¹⁴ and affecting helix formation.¹⁵ Consequently, the study of the ability of salt bridges to interact with other moieties is fundamental for understanding the structural and functional roles that they play. This aspect has been scarcely analyzed in the literature because, apart from the $\text{sb}-\pi$ investigation referenced above,¹⁰ limited investigations have been devoted to the study of ternary complex systems involving salt bridges and aromatic compounds;^{16–19} primarily, the focus was limited to the influence of the salt bridge upon the cation– π interaction or comparisons between the strength of the cation– π and the salt bridge.

In this manuscript, we analyze the possibility of noncovalent contacts between the salt-bridge and lone-pair donors because we have serendipitously observed this interaction between malonate oxygen atoms in the solid-state crystal structure of a Cu(II) malonate perchlorate complex. We define and name this new contact as a “lone pair–salt-bridge” interaction, and we theoretically analyze the strength of this interaction, both in models and in the crystal structure. Moreover, the synthesis, structural determination, and routine physicochemical analyses of a Cu(II) malonate complex, $\{(C_5H_6N_2Cl)_{12}[\text{Cu}(1)(C_3H_2O_4)_2][\text{Cu}(2)(C_3H_2O_4)_2(H_2O)_2][\text{Cu}(4)(C_3H_2O_4)_2][\text{Cu}(3)(C_3H_2O_4)_2(H_2O)_2](\text{ClO}_4)_4\}_n$ (**1**) [where $C_5H_6N_2Cl$ = protonated 2-amino-5-chloropyridine, $C_3H_2O_4$ = malonic acid, and ClO_4^- = perchlorate] are described. The single-crystal X-ray structural analysis of **1** revealed remarkable supramolecular architecture guided by various weak forces like hydrogen bonding, lone pair– π , $\pi-\pi$, salt-bridge– π , anion– π , chloride– π and the newly observed, lone pair–salt-bridge interactions. Most of the aforementioned weak forces are further combined to form an remarkable infinite network, which can be best described as [...]–(sb– π)+(lp– π)+(Cl– π)/(sb– π)+(lp– π)/ $\pi-\pi$ /(sb– π)+(Cl– π)/(lp–sb)+(sb– π)/ $\pi-\pi$...]. This unique combination of weak forces is the first report in any crystalline structures of synthetic molecules. An in-depth structural analysis of the present complex is fully described here.

2. EXPERIMENTAL SECTION

2.1. Physical Measurements. IR spectra were recorded on a Perkin-Elmer RXI FT-IR spectrophotometer with the sample prepared as a KBr pellet in the range 4000–600 cm^{-1} . Elemental analyses (C, H, N) were performed on a Perkin-Elmer 240C elemental analyzer.

2.2. Materials. All reactions were carried out under aerobic conditions and with water as the solvent. Malonic acid (Aldrich), copper(II) perchlorate hexahydrate, and 2-amino-5-chloropyridine (Aldrich) were used as received. Freshly boiled, doubly distilled water was used throughout the present investigation.

2.3. Synthesis of Compound 1. Copper(II) perchlorate hexahydrate (0.370 g, 1.0 mmol) dissolved in 25 mL of water was allowed to react with malonic acid (0.208 g, 2.0 mmol) in water (25 mL) at $\sim 60^\circ\text{C}$, resulting in a clear blue solution. A warm aqueous solution (20 mL) of 2-amino-5-chloropyridine (0.504 g, 4.0 mmol) was added dropwise to the above solution with continuous stirring. The reaction mixture thus obtained was further heated to $\sim 60^\circ\text{C}$ for 1 h with continuous stirring. The solution was then cooled to room temperature, filtered, and left unperturbed for crystallization. After a few weeks, rectangular, blue-colored single crystals suitable for X-ray analysis were obtained. The crystals were collected by filtration,

washed with cold water and dried in air (yield: 60%). Anal. calcd for $C_{84}H_{96}N_{24}O_{52}Cl_{16}Cu_4$: C, 32.56; H, 3.12; N, 10.85%. Found: C, 32.57; H, 3.11; N, 10.83%. Main IR absorption bands observed for **1** (KBr pellet, cm^{-1}) are: 3319 (b), 3088 (s), 1681 (b), 1621 (s), 1586 (s), 1479 (s), 1423 (b), 1380 (s), 1249 (s), 1091 (b), 977 (s), 836 (s), 741 (s), 666 (s).

2.4. X-ray Crystal Structure Determination of 1. X-ray diffraction data collection was carried out on a Bruker SMART APEX CCD diffractometer with graphite-monochromated Mo $\text{K}\alpha$ radiation ($\lambda = 0.71073 \text{ \AA}$). The data were processed using SAINT²⁰ and corrected for absorption using SADABS.²¹ The crystal structures were solved by direct methods using SHELXS-97²² and refined by full-matrix least-squares on F^2 with SHELXL-97.²² Other calculations were carried out using the SHELXTL package.²² The H atoms other than those bonded to O were placed in geometrically idealized positions and constrained to ride on their parent atoms. Hydrogen atoms bonded to the water O atoms were found by difference Fourier methods and refined isotropically with restraints on their geometry. The O atoms of one of the perchlorate ions were disordered over two sites, whose occupancies were constrained to sum to unity. Data collection and refinement parameters for complex **1** are summarized in Table S1. (See the Supporting Information.)

3. RESULTS AND DISCUSSION

3.1. Crystal Structure Description of 1. Compound **1** crystallizes in the triclinic space group $P\bar{1}$ with the asymmetric

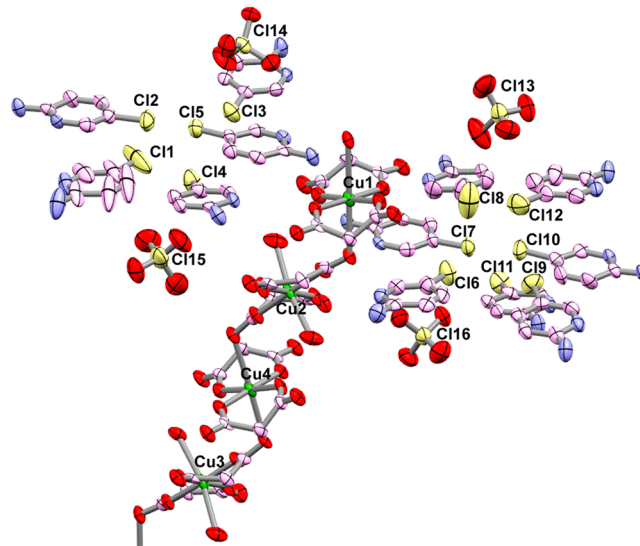


Figure 1. ORTEP diagram of **1** with 50% ellipsoidal probability. Only selected atoms are numbered for clarity. Hydrogen atoms are omitted for clarity. Only one set of oxygen atoms for the disordered perchlorate anion is shown. Color code: Cu, green; O, red; N, blue; C, light purple; chlorine, yellow.

unit consisting of one tetranuclear anionic $\{[\text{Cu}(1)\text{C}_3\text{H}_2\text{O}_4)_2][\text{Cu}(2)(\text{C}_3\text{H}_2\text{O}_4)_2(\text{H}_2\text{O})_2][\text{Cu}(4)\text{C}_3\text{H}_2\text{O}_4)_2][\text{Cu}(3)(\text{C}_3\text{H}_2\text{O}_4)_2(\text{H}_2\text{O})_2]\}^{8-}$ unit containing 4 crystallographically independent copper atoms, 12 protonated 2-amino-5-chloropyridine molecules, and 4 perchlorate anions, among which one perchlorate anion is disordered. The full copper(II) malonate structure consists of infinite 1D polymeric chains. A representative ORTEP diagram is shown in Figure 1. Selected bond lengths, angles, and supramolecular interactions are listed

Table 1. Geometrical Parameters (\AA , deg) for Lone-Pair $\cdots\pi$, Anion $\cdots\pi$, and Chloride $\cdots\pi$ Interactions in **1**^a

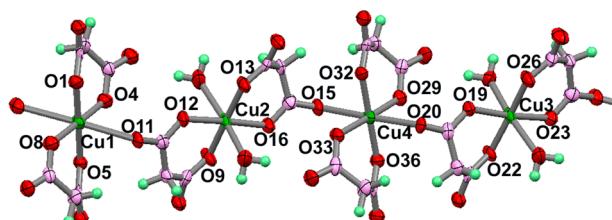
Y–X(I) \cdots Cg(J) ^a	X \cdots Cg	Y \cdots Cg	Y–X \cdots Cg	X–Perp	symmetry
Lone-Pair $\cdots\pi$ Contacts					
C(4)–O(6) \cdots Cg(15)	3.521(4)	3.696(6)	88.2(3)	3.051	1 – x, 1 – y, –z
C(7)–O(10) \cdots Cg(16)	3.509(4)	3.858(6)	96.9(3)	3.071	1 – x, 1 – y, –z
C(18)–O(25) \cdots Cg(12)	3.458(4)	3.926(6)	103.3(3)	3.020	2 – x, 2 – y, 1 – z
Anion $\cdots\pi$ Contacts					
Cl(13)–O(38) \cdots Cg(20)	3.941(5)	4.612(3)	109.22(19)	3.494	x,y,z
Cl(15)–O(45B) \cdots Cg(9)	3.703(3)	4.772(3)	108.41(16)	2.944	x,y,z
Chloride $\cdots\pi$ Contacts					
C(48)–Cl(5) \cdots Cg(12)	3.548(2)	3.878(4)	87.48(16)	3.453	x,y,z
C(58)–Cl(7) \cdots Cg(16)	3.720(3)	4.103(5)	89.99(16)	3.497	x,y,z
C(73)–Cl(10) \cdots Cg(17)	3.726(3)	3.520(5)	69.65(16)	3.529	x,y,z

^aCg(J) denotes centroid of Jth ring; Ring (9) [N(2)/C(25)/C(26)/C(27)/C(28)/C(29)]; Ring (12) [N(8)/C(40)/C(41)/C(42)/C(43)/C(44)]; Ring (15) [N(14)/C(55)/C(56)/C(57)/C(58)/C(59)]; Ring (16) [N(16)/C(60)/C(61)/C(62)/C(63)/C(64)]; Ring (17) [N(18)/C(65)/C(66)/C(67)/C(68)/C(69)]; Ring (20) [N(24)/C(80)/C(81)/C(82)/C(83)/C(84)].

Table 2. Geometrical Parameters (\AA , deg) for $\pi\cdots\pi$ Interactions in **1**^a

Cg(I) ^a \cdots Cg(J)	Cg \cdots Cg	dihedral angle	symmetry
Cg(9) \rightarrow Cg(18)	3.928(3)	6.8(3)	1 – x, 1 – y, –z
Cg(10) \rightarrow Cg(20)	3.808(3)	5.6(2)	1 – x, 1 – y, –z
Cg(11) \rightarrow Cg(15)	3.629(2)	4.3(2)	1 – x, 1 – y, 1 – z
Cg(11) \rightarrow Cg(17)	3.685(3)	2.7(2)	–1 + x, y, z
Cg(14) \rightarrow Cg(19)	3.779(3)	0.5(2)	2 – x, 1 – y, 1 – z
Cg(17) \rightarrow Cg(18)	3.982(3)	2.7(2)	x, y, z

^aCg(I) denotes centroid of Ith ring; Ring (9) [N(2)/C(25)/C(26)/C(27)/C(28)/C(29)]; Ring (10) [N(4)/C(30)/C(31)/C(32)/C(33)/C(34)]; Ring (11) [N(6)/C(35)/C(36)/C(37)/C(38)/C(39)]; Ring (14) [N(12)/C(50)/C(51)/C(52)/C(53)/C(54)]; Ring (15) [N(14)/C(55)/C(56)/C(57)/C(58)/C(59)]; Ring (17) [N(18)/C(65)/C(66)/C(67)/C(68)/C(69)]; Ring (18) [N(20)/C(70)/C(71)/C(72)/C(73)/C(74)]; Ring (19) N(22)/C(75)/C(76)/C(77)/C(78)/C(79); Ring (20) N(24)/C(80)/C(81)/C(82)/C(83)/C(84).

**Figure 2.** Tetrameric copper building block of **1** which forms 1-D polymeric chains.

in Tables S2–S4 in the Supporting Information and Tables 1 and 2, respectively.

Tetranuclear unit consists of alternating $[\text{Cu}(\text{C}_3\text{H}_2\text{O}_4)_2]^{2-}$ and $[\text{Cu}(2)(\text{C}_3\text{H}_2\text{O}_4)_2(\text{H}_2\text{O})_2]^{2-}$ units bridged by malonate oxygen atoms. In **1**, there are two types of Cu(II) centers exhibiting two different geometric arrangements around the Cu(II) atoms. In the $[\text{Cu}(\text{C}_3\text{H}_2\text{O}_4)_2]^{2-}$ units, the coordination geometry around the copper(II) ion can be best described as a distorted square-pyramid with a $\text{CuN}_2\text{O}_2\text{O}'$ chromophore. In the $[\text{Cu}(2)(\text{C}_3\text{H}_2\text{O}_4)_2(\text{H}_2\text{O})_2]^{2-}$ units, the coordination geometry around the copper(II) ion is a distorted octahedron, forming a $\text{CuN}_2\text{O}_2\text{O}'$ chromophore. The basal plane for all of the copper atoms is formed by malonate oxygen atoms. In the $[\text{Cu}(\text{C}_3\text{H}_2\text{O}_4)_2]^{2-}$ units, the apical positions are occupied by malonate oxygen atoms from diaqua bis malonato units, and in

the $[\text{Cu}(2)(\text{C}_3\text{H}_2\text{O}_4)_2(\text{H}_2\text{O})_2]^{2-}$ units, the axial positions are occupied by water molecules. In both of the units, axial bonds are significantly longer than equatorial bonds, as expected for Jahn–Teller distorted d⁹ system. No unusual bond lengths and bond angles are found for the chelated ligands in **1** compared with other malonate-containing copper(II) compounds consisting of similar $\text{CuN}_2\text{O}_2\text{O}'$ chromophores.²³ It is observed that in square-planar copper(II) complexes the metal ion is involved in weak interactions at the apical position with another atom of a neighboring molecule, forming dimeric units or polymeric chains having equatorial–apical bridges.²⁴ We have also observed such polymerization of copper units linked through malonate bridges in the course of our studies.^{10,25–28} In **1**, the copper units polymerize through malonate bridges to form infinite 1D chains, which are further strengthened by O18–H18P \cdots O3, O17–H17P \cdots O34, O28–H28P \cdots O30, and O27–H27P \cdots O7 hydrogen bonds. Within these chains, the tetrameric Cu1–Cu2–Cu4–Cu3 unit acts as the building block or repeat unit (Figure 2). It is also interesting to note that axial and equatorial bond lengths and malonate bite angles in different copper malonate moieties of the tetrameric repeat unit vary significantly (Tables S2 and S3 in the Supporting Information).

These 1D chains are interlinked side-by-side by strong self-complementary O18–H18O \cdots O2 and O28–H28O \cdots O31 hydrogen bonds to form a 2D sheet-like structure that constitutes the [111] plane of the complex (Figure S1 in the Supporting Information). Finally, these 2D sheets are interlocked by several hydrogen bonds with various strengths to generate the overall 3D structure of **1**. (See Table S4 in the Supporting Information.)

Each bis(malonato)–copper(II) unit containing Cu(1) and Cu(4) recognizes two chloroaminopyridinium cations ($\text{C}_5\text{H}_6\text{N}_2\text{Cl}^+$) through doubly coordinated carboxylate ends, leading to R₂²(8) hydrogen bonding motifs involving the hydrogen bonds N15–H15N \cdots O6, N16–H16N \cdots O5, N8–H8N \cdots O1, N7–H7N \cdots O2 and N17–H17N \cdots O35, N18–H18N \cdots O36, N22–H22N \cdots O32, N21–H21N \cdots O31, respectively (Figure 3). The $[\text{Cu}(2)(\text{C}_3\text{H}_2\text{O}_4)_2(\text{H}_2\text{O})_2]^{2-}$ unit similarly recognizes four chloroaminopyridinium cations ($\text{C}_5\text{H}_6\text{N}_2\text{Cl}^+$) involving the hydrogen bonds N2–H2N \cdots O10, N1–H1N \cdots O9, N10–H10N \cdots O11, N9–H9N \cdots O12, N11–H11N \cdots O13, N12–H12N \cdots O14, N19–H19N \cdots O16, and N20–H20N \cdots O15. In contrast, although the $[\text{Cu}(3)(\text{C}_3\text{H}_2\text{O}_4)_2(\text{H}_2\text{O})_2]^{2-}$ unit recognizes four chloroaminopyridini-

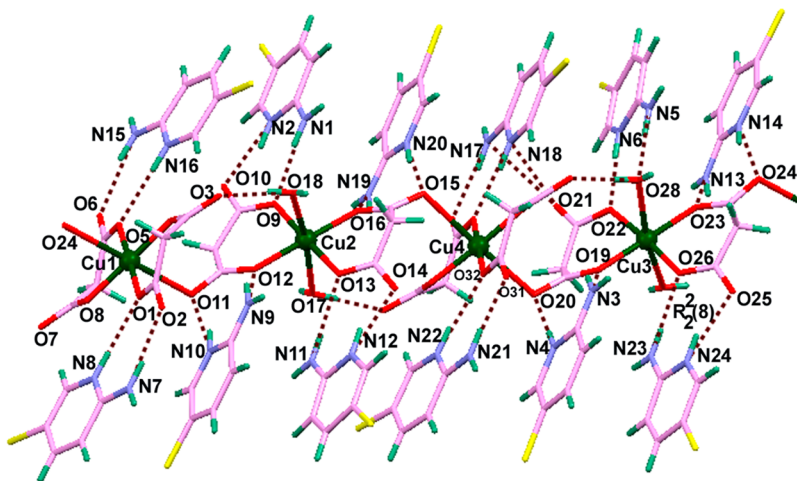


Figure 3. Recognition of the chloroaminopyridinium cations by the tetrameric copper unit of **1** through various hydrogen bonds. Viewed along *b* axis. Color code: Cu, green; O, red; N, blue; C, light purple; H, aquamarine; Cl, yellow.

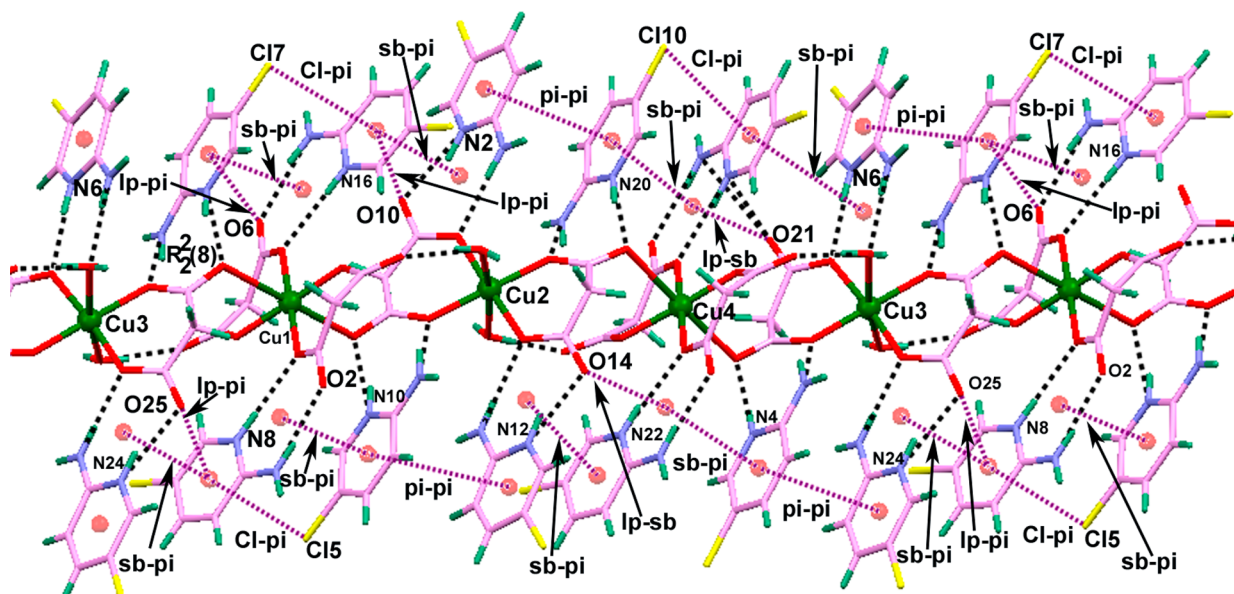


Figure 4. Supramolecular network of the weak forces in **1**. Viewed along *b* axis. Color code: Cu, green; O, red; N, blue; C, light purple; H, aquamarine; Cl, yellow.

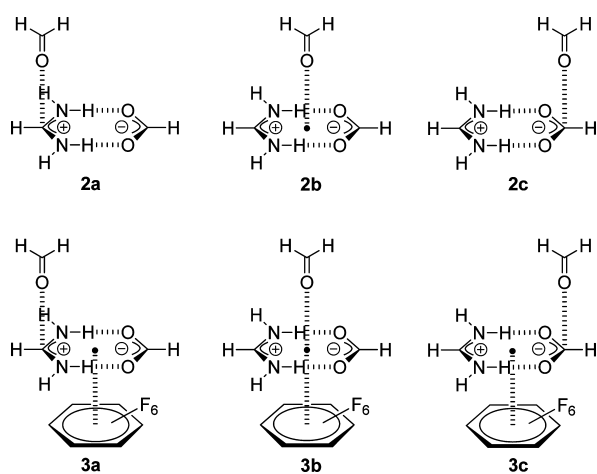


Figure 5. Complexes **2a–c** and **3a–c** studied in this work.

Table 3. Interaction Energies without and with the Basis Set Superposition Error (*E* and *E*_{BSSE}, respectively, in kcal/mol) and Distances from the O Atom to the Molecular Plane at the BP86-D3/def2-TZVP Level of Theory

complex	<i>E</i>	<i>E</i> _{BSSE}	<i>R</i>
2a	-1.30	-1.17	2.825
2b	-0.12	-0.01	2.825
2c	1.54	1.63	2.825
3a	-1.23 ^a	-1.11	2.750
3b	-0.82 ^a	-0.70	2.750
3c	1.13 ^a	1.24	2.750

^aValues computed considering the sb-π complex previously formed; therefore, only the lp-sb is evaluated.

nium cations, it does not fully utilize all four different carboxylate ends. Three of the cations are attached to Cu(3) unit by N13-H13N...O23, N14-H14N...O24, N4-H4N...O20, N3-H3N...O19, N23-H23N...O26, and N24-

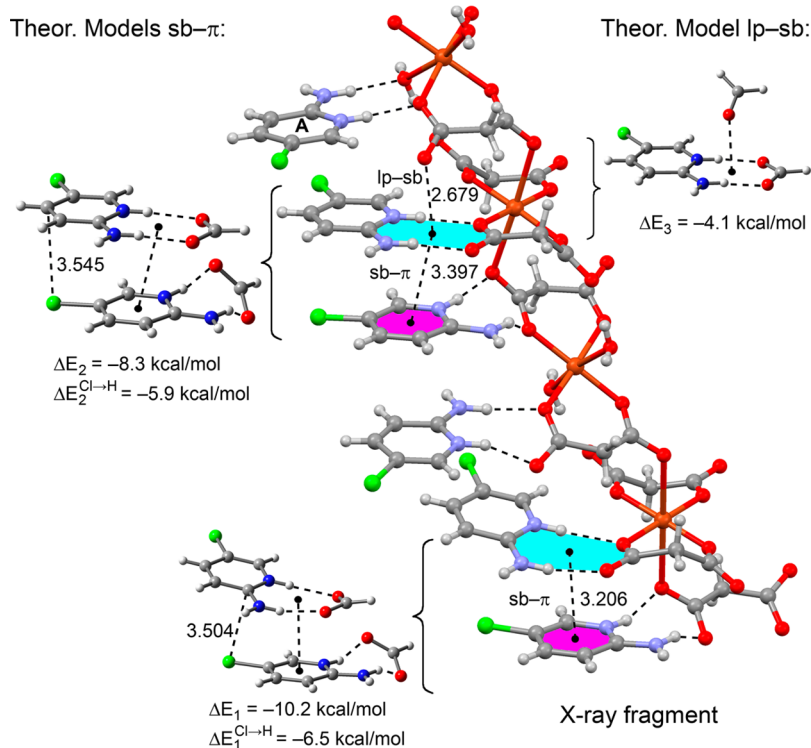


Figure 6. Crystal fragment used to perform the theoretical study and several models used to evaluate the interactions. Distances are in angstroms.

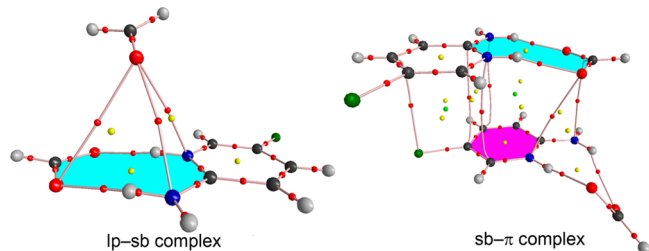


Figure 7. Distribution of the critical points in two crystal fragments of compound **1** are shown, corresponding to the lp \cdots sb (left) and sb \cdots π (right) interactions. Bond-, ring-, and cage-critical points are represented by red, yellow, and blue spheres, respectively. The bond paths are also indicated.

Table 4. CSD Reference Codes of X-ray Structures Exhibiting lp \cdots sb Interactions^a

CSD CODE	lp donor	lp \cdots sb distance
COSFUM ³³	O	3.025
DUSKOS ³⁴	O	2.592
EBAZOY01 ³⁵	F	2.911
EBOOKIP ³⁶	O	3.095
EFALII ³⁷	F	3.099
HATTIG ³⁸	O	3.202
KUSTEY ³⁹	F	3.093
KUSVEA ⁴⁰	F	3.064
NUQVEB ⁴¹	O	3.027
TETXOF ⁴²	Cl	3.427
VABLOZ ⁴³	F	3.300

^alp donor atom and the distance (angstroms) from it to the salt-bridge centroid are also given.

H24N \cdots O25 hydrogen bonds. The fourth cation is attached in a somewhat different manner and involves one axial oxygen

atom (O28) through N6 \cdots H6N \cdots O22 and N5 \cdots HSN \cdots O28 hydrogen bonds. Surprisingly, O21 remains uncoordinated in this recognition process. In previous structures, we always observed recognition of aminopyridinium cations by the carboxylate ends of the copper malonate units; therefore, the recognition seen in **1** is unusual.^{25–28} There are two different sets of six choloroaminopyridinium cations amounting to 12 independent such cations.

The uncoordinated malonate oxygen atom O21 of the Cu(3) unit is found to be engaged in an unusual contact with the planar salt bridge (sb) formed by the malonate and the choloroaminopyridinium cation [The ring is defined by the atoms N(18)/C(65)/C(66)/C(67)/C(68)/C(69).] We observe a very interesting supramolecular contact between lone pair of O21 and the centroid of a planar salt bridge. The distance between the centroid of the salt bridge and O21 is 2.679 Å, and the angle C(15) \cdots O(21) \cdots Cg(sb) is 113.86°. The shortest distances reflecting this interaction are O21 \cdots N18 = 3.022(5) and O21 \cdots N17 = 3.057(5) Å, which are slightly below the sum of the corresponding van der Waals radii (sum of van der Waals radii of O and N is 3.07 Å).²⁹ The C(15) \cdots O(21) \cdots Cg(sb) angle of 113.86° suggests a significant involvement of the oxygen lone pair with the salt bridge, as proposed by Egli et al. previously in the case of a lone pair interacting with an aromatic π system.³⁰ We define and name this novel stacking phenomenon as a lone-pair–salt-bridge interaction. It is virtually unexplored and quite different to the so-far well-studied cation– π , anion– π , and lone pair– π interactions. This novel interaction will be dealt with in detail in the theoretical part of the paper. The lone pair of the malonate oxygen atom, O21, is so strongly engaged with the salt bridge that it is unavailable for hydrogen bonding. Because of the unavailability of O21, the axial oxygen atom (O28) in the [Cu(3)(C₃H₂O₄)₂(H₂O)]²⁺ unit becomes more important, leading

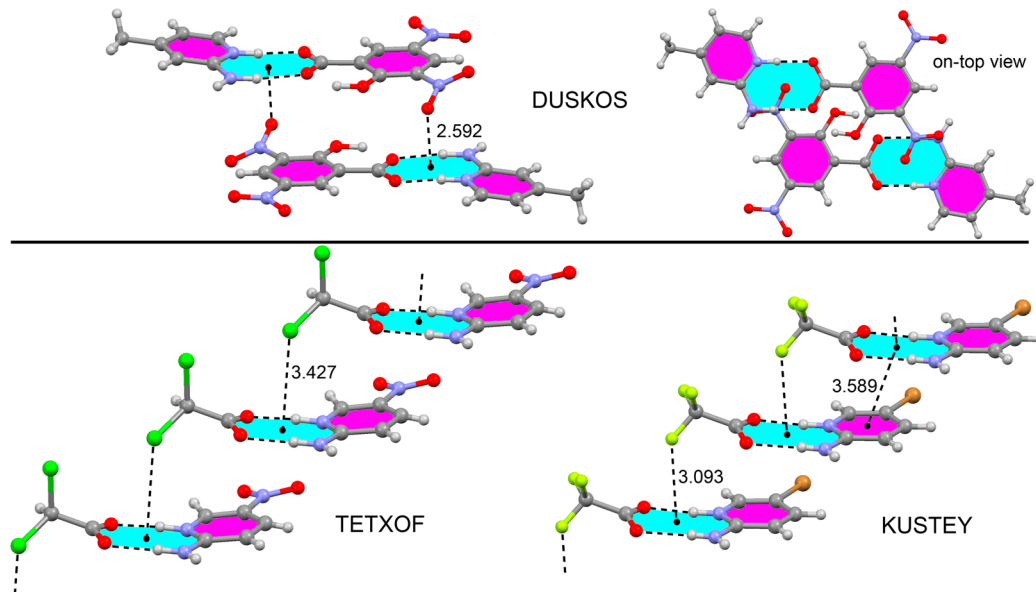


Figure 8. Fragments of three X-ray structures retrieved from the CSD (the codes are indicated). Distances are in angstroms.

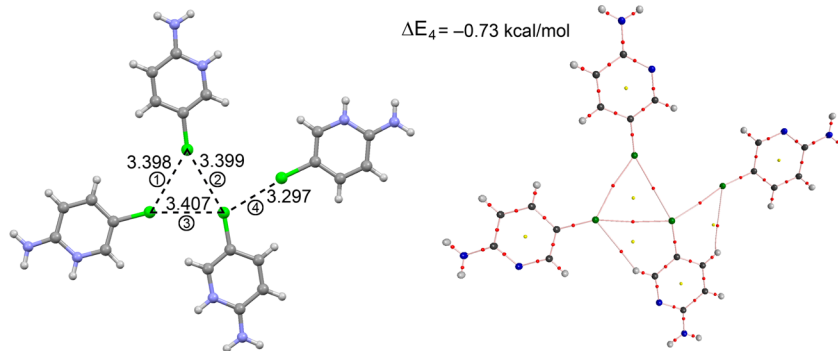


Figure 9. Left: X-ray fragment showing the almost perfect regular triangle formed by three Cl···Cl halogen bonding interactions and the additional Cl···Cl interaction. The interaction energy of a neutral model is also indicated. Right: The distribution of the critical points is shown. Bond-, ring- and cage-critical points are represented by red, yellow, and blue spheres, respectively. The bond paths are also indicated.

to a different recognition process for one of the choloroaminopyridinium cations.

Another such lone-pair–salt-bridge interaction is also observed, where the lone pair of O14 is involved in the interaction with the salt bridge formed by the choloroaminopyridinium cation defined by the atoms N22/C75/C76/C77/C78/C79] and malonate. The distance between centroid of the salt bridge and O14 is 2.831 Å, and the angle C(10)–O(14)–Cg(sb) is 117.75°. In both the cases, the aforementioned choloroaminopyridinium rings are also involved in π interaction with their nearest salt bridges. Therefore, the lone pair···salt-bridge and salt-bridge··· π interactions are operating simultaneously (Figure 4).

In addition, there exists three distinct lone pair··· π (aromatic) interactions involving the malonate oxygen atoms O25, O10, and O6 operating in 1, details of which are summarized in Table 1 and shown in Figure 4. Some of the chloride atoms of choloroaminopyridinium cations are found to participate in Cl··· π interactions³¹ and most interestingly, in a single step, three weak forces, namely, Cl(7)··· π , sb··· π , and lone pair [O(6)]··· π operate simultaneously, revealing their subtle role in organizing molecules in the solid state. Geometric parameters of such chloride– π interactions are summarized in Table 1 and

shown in Figure 4. Additionally, anion– π interactions involving perchlorate oxygen atoms and π ··· π interactions between suitably stacked choloroaminopyridinium cations are worth mentioning. Interplay of π ··· π stacking interactions with other forces are shown in Figure 4, and their geometrical parameters are summarized in Table 2. Anion– π interactions (geometrical parameters are summarized in Table 2) act in unison with relatively stronger hydrogen bonds to stitch 2D copper malonate sheets along the *ab* direction.

A series of salt-bridge··· π contacts have been found to operate on either side of the infinite 1D polymeric chain formed by the different Cu(II) malonate units. We first observed the formation of such salt bridge··· π contacts in the copper complex, namely, $\{(C_5H_7N_2)_6[Cu(C_3H_2O_4)_2(H_2O)_2] \cdot [Cu(C_3H_2O_4)_2](PF_6)_2\}_n$ (1) [$C_5H_7N_2$ = protonated 2-amino-pyridine, $C_3H_2O_4$ = malonic acid]. We also provided an in-depth structural and theoretical investigation to confirm its acceptance as a new supramolecular moiety.²³ In 1, these salt-bridge··· π contacts along with other weak forces like lone-pair··· π , π ··· π , chloride··· π , and lone-pair···sb generate an amazing supramolecular infinite network, which can be described as $[...(sb-\pi)+(lp-\pi)+(Cl-\pi)/(sb-\pi)+(lp-\pi)/\pi-\pi/(sb-\pi)+(Cl-\pi)/(lp-sb)+(sb-\pi)/\pi-\pi...]_n$ (Figure 4).

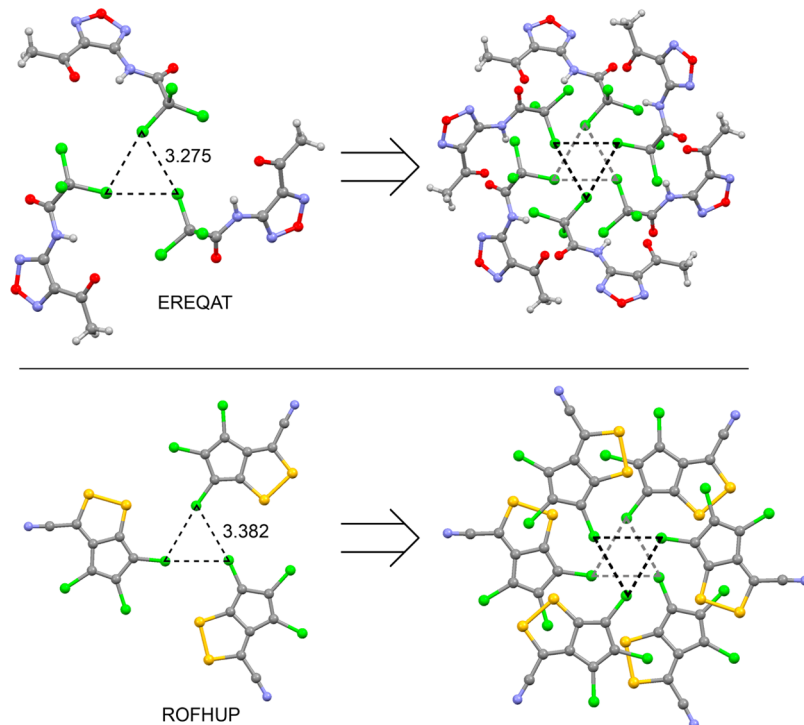


Figure 10. X-ray structures exhibiting ternary $\text{Cl}\cdots\text{Cl}$ interactions.

This intricate network of weak forces is observed for the first time in any crystalline structure. Such an elegant network of weak noncovalent forces submits a challenge for the theoretical chemists and crystal engineers to investigate their mutual influences in a competitive environment and structure-directing potentialities.

3.2. Theoretical Study. Interactions Involving the Salt Bridge. We have analyzed several aspects of the interesting noncovalent interactions observed in the solid-state structure of compound **1** using theoretical DFT-D3 calculations that include the latest available correction for dispersion effects. (See the Supporting Information for theoretical methods.) Previously, it was convenient to analyze both the energetic and geometric suitability of a salt-bridge moiety to interact with lone-pair donor molecules. Moreover, because in the X-ray structure the salt bridge that participates in the $\text{lp}\cdots\text{sb}$ interaction also establishes a $\text{sb}\cdots\pi$ interaction, we have evaluated the $\text{lp}\cdots\text{sb}$ interaction in the presence of an electron-deficient ring (hexafluorobenzene) located at the opposite side of the salt bridge to establish the influence of a $\text{sb}\cdots\pi$ on the $\text{lp}\cdots\text{sb}$ interaction. As a model for the salt bridge, we have used the pair formed by the formate anion and the formamidinium cation. The interaction energies of complexes **2a–c** and **3a–c** (Figure 5) are summarized in Table 3. It should be noted that we have optimized the geometries of the salt bridge and the formaldehyde as isolated moieties and fixed these geometries in the complexes. Following this, only the distance between the interacting parts was optimized. The full optimization of these ternary systems without these constraints yields a totally different organization of the molecules, which is not the intention of this work. The optimization of the distance was performed for **2b** and **3b**, namely, $\text{lp}\cdots\text{sb}$ and $\text{lp}\cdots\text{sb}\cdots\pi$ complexes, and, subsequently, the H_2CO molecule moved to the positive and negative parts of the salt bridge while

maintaining a constant distance between the salt bridge and the interacting molecule.

From this study, it is clear that the cationic end of the salt bridge is a better lone pair acceptor, as expected.¹⁰ In addition, when the oxygen atom of the H_2CO is pointing to the center of the salt bridge, the interaction energy is negligible. This is probably due to a compensating effect of two opposing charge–dipole interactions. The repulsion observed in complex **2c**, where the oxygen atom is located over the negative part of the salt bridge, is also small. The interaction energies of complexes **3a–c** are similar to those computed for **2a–c**, indicating that the presence of the electron-deficient aromatic ring at the opposite part of the salt bridge has a very modest effect on the strength of the $\text{lp}\cdots\text{sb}$ interaction.

Taking into consideration these preliminary calculations, we have analyzed the noncovalent interactions observed in the solid-state structure of compound **1** using the crystallographic coordinates. The recognition of 2-amino-5-chloropyridinium cations by the tetrameric copper unit of **1** leads to the formation of several salt bridges, as previously described in the analysis of the solid-state structure. Some of them participate in $\text{sb}\cdots\pi$ and $\text{lp}\cdots\text{sb}$ interactions, and we have focused our attention on describing the energetic features of these complexes. The fragment of the crystal structure studied and the computational models are shown in Figure 6. It is interesting to note that only two salt-bridge moieties are almost planar, which are highlighted in blue in Figure 6. Both planar salt bridges are involved in $\text{sb}\cdots\pi$ interactions that we have evaluated using formate instead of malonate to simplify the theoretical model. Both $\text{sb}\cdots\pi$ complexes are characterized by short equilibrium distances and the presence of an additional $\text{Cl}\cdots\pi$ interaction that contributes to the binding energy. We have evaluated the interaction energies of both complexes, which are $\Delta E_1 = -10.2 \text{ kcal/mol}$ and $\Delta E_2 = -8.3 \text{ kcal/mol}$. (See Figure 6.) These energies also include the contribution of

the $\text{Cl}\cdots\pi$ interaction. To evaluate it, we have computed the binding energies of both complexes, replacing the chlorine atom by a hydrogen atom, and we have denoted them as $\Delta E_1^{\text{Cl}\rightarrow\text{H}}$ and $\Delta E_2^{\text{Cl}\rightarrow\text{H}}$. These values are also included in Figure 6, and by comparison with ΔE_1 and ΔE_2 values, it can be deduced that the contribution of the $\text{Cl}\cdots\pi$ interaction ranges from -3.7 to -2.4 kcal/mol, and the $\text{sb}\cdots\pi$ interaction is around -6 kcal/mol for both complexes. After describing the $\text{lp}\cdots\text{sb}$ interaction, it should be emphasized that all protonated 2-amino-5-chloro-pyridine moieties in the crystal structure establish a salt-bridge interaction by means of a double hydrogen bond, with both oxygen atoms of the carboxylate group belonging to the malonate, apart from one moiety that interacts with only one oxygen atom of the malonate and the oxygen atom of a water molecule, coordinated to the copper metal center. (See the aminopyridine labeled as "A" at the top of Figure 6.) Interestingly, the other oxygen of the malonate is used to form the $\text{lp}\cdots\text{sb}$ interaction, and it is located at 2.68 \AA from the centroid of the salt bridge. To evaluate the interaction energy, we have used formaldehyde as a model of the "free" oxygen atom of malonate (Figure 6, top right). The computed interaction energy is $\Delta E_3 = -4.1$ kcal/mol, which is considerably more favorable than the computed value in the preliminary study. This is clearly due to the directionality of the $\text{lp}\cdots\text{sb}$ observed in the crystal structure.

The Bader's theory of "atoms in molecules" (AIM),³² which provides an unambiguous definition of chemical bonding, has been used to further describe the noncovalent interactions described above for compound **1**. The AIM theory has been successfully applied to characterize and for a better understanding of a great variety of noncovalent interactions. The representation of critical points and bond paths computed for the $\text{lp}\cdots\text{sb}$ and $\text{sb}\cdots\pi$ complexes is depicted in Figure 7. The $\text{lp}\cdots\text{sb}$ interaction is characterized by the presence of three bond critical points that connect the oxygen atom of the carbonyl group to one oxygen and two nitrogen atoms of the salt bridge (Figure 7, left). The interaction is further characterized by the presence of two ring critical points. Interestingly, the bond paths indicate that the interaction is not with the hydrogen atoms of the saltbridge; instead, it is with three heteroatoms of the salt bridge. The $\text{sb}\cdots\pi$ interaction is characterized by the presence of four bond critical points connecting several carbon and nitrogen atoms of the aromatic ring with several atoms of the salt bridge (Figure 7, right) and one critical point connecting the exocyclic amino group with the carbon atom of the formiate. Moreover, this interaction is further described by the presence of several ring- and one cage-critical points. In addition, the $\text{Cl}\cdots\pi$ interaction is characterized by the presence of one bond-critical point that connects the chlorine atom with one carbon atom of the pyridine ring (Figure 7).

The presence of the aforementioned critical points confirms the existence of the noncovalent interactions described above in the solid-state structure of compound **1**, which have been energetically evaluated by DFT calculations; these supramolecular bonding interactions certainly influence the solid-state architecture of the coordination polymer.

To gain further insight into the $\text{lp}\cdots\text{sb}$ interaction and its relative importance in the solid state, we have analyzed the Cambridge Structural Database, which is a big storehouse of geometrical information. For the search, we have used protonated 2-aminopyridine derivatives for the cationic part and carboxylates for the anionic part of the salt bridge. We have

found 225 X-ray structures exhibiting the previously defined salt bridge, and only 11 structures present a clear $\text{lp}\cdots\text{sb}$ interaction. It should be mentioned that we have only selected those hits presenting a nearly planar salt bridge and a short $\text{lp}\cdots\text{sb}$ contact. The structures and some geometric details are summarized in Table 4. This reduced number of hits can be related to the small interaction energy associated with this interaction. However, in some structures, it has a very relevant role in the final architecture of the solid-state structure. Three selected examples are represented in Figure 8, where the salt bridge has been highlighted in blue and three different lone pair donors are shown. The DUSKOS structure is interesting because it forms dimers in the solid state where two complementary $\text{lp}\cdots\text{sb}$ interactions are established. The lp donor is an oxygen atom of a nitro group that is very close to the salt-bridge centroid (2.59 \AA) and, interestingly, the nitro group is not coplanar with the aromatic ring; instead, it is somewhat rotated (28°) to favor the interaction with the salt bridge. In addition, the interacting oxygen atom is located almost exactly over the centroid of the salt bridge, as can be observed in the on-top representation (see Figure 8, top right). The other two structures (TETXOF and KUSTEY) present a similar organization in the solid state, forming infinite ladders characterized by the presence of relevant $\text{lp}\cdots\text{sb}$ interactions. In the KUSTEY structure, an $\text{sb}\cdots\pi$ interaction is observed generating an $\text{lp}\cdots\text{sb}\cdots\pi$ assembly, as it is also observed in the title compound.

In conjunction, the title compound synthesized and described herein and the aforementioned structures retrieved from the CSD search represent clear examples where this previously unnoticed $\text{lp}\cdots\text{sb}$ noncovalent interaction plays a relevant role in the crystal packing. For instance, it is particularly relevant that the malonate that participates in the $\text{lp}\cdots\text{sb}$ interaction in **1** has a different binding mode with the adjacent protonated aminopyridine moiety, where the participation of a coordinated water molecule to liberate an oxygen atom of the malonate is directly related to the presence of the salt bridge and the formation of the interaction. Similarly, in DUSKOS structure, the planarity of one nitro group is lost to facilitate the interaction with the salt bridge.

Halogen Bonding Interactions. Another interesting aspect of the crystal structure is the presence of halogen bonding interactions involving the chlorine substituent of the pyridine ring. In Figure 9 we show a fragment of the X-ray structure where the halogen bonds are present. Curiously, an almost perfect equilateral triangle is formed by means of three halogen bonds, labeled as 1–3. Furthermore, a fourth 2-amino-5-chloropyridine ring is also present, forming an additional halogen bonding interaction (labeled as 4). To the best of our knowledge, the three-center halogen bonding involving three halogen atoms located at the vertices of a regular triangle has not been studied theoretically before.⁴⁴ In contrast, bifurcated halogen bonds have been previously described and analyzed theoretically. Because the halogen bond donor is chlorine, which has a very small σ -hole, the $\text{Cl}\cdots\text{Cl}$ interactions are expected to be energetically modest. As a matter of fact, the computed interaction energy of the quaternary assembly shown in Figure 9, where neutral aminopyridine molecules have been used to avoid the electrostatic repulsion between the cationic moieties, is only $\Delta E_4 = -0.73$ kcal/mol. The AIM analysis, which is also shown in Figure 9 (right) confirms the existence of the $\text{Cl}\cdots\text{Cl}$ interactions. Each interaction is characterized by the presence of a bond critical point connecting both chlorine

atoms. In the case of the three-center halogen bond, the interaction is further characterized by the presence of a ring critical point located at the geometrical center of the triangle. Secondary C–H···Cl hydrogen bonds are also established.

Although the three-center halogen bond that has very modest interaction energy has not been previously studied theoretically, there are several experimental works where this interaction has been described. For instance, Seregin et al.⁴⁵ have reported that the reaction of diacetyl furoxan with trichloroacetonitrile in ionic liquids at 80 °C yielded an unexpected compound, which is *N*-(4-acetyl-1,2,5-oxadiazol-3-yl)-2,2,2-trichloroacetamide. Because of Cl···Cl contacts (Figure 10, top), molecules in the solid state are assembled into tubes directed along the crystallographic axis *c* and parallel to the crystallographic plane *ab*. The trimer connected by the short Cl···Cl interactions, while Cl···O contacts between “layers” assemble molecules into an infinite tube-like structure. Another interesting example is shown in Figure 10, bottom. Unexpectedly, the X-ray diffraction analysis of 4,5,6-trichlorocyclopenta-1,2-dithiole-3-carbonitrile revealed that the molecules are packed in layers with strong intermolecular attractions, as evidenced by the short distances between the Cl atoms of molecules belonging to the same layer (Cl–Cl, 3.38 Å).⁴⁶ The interaction between the layers is basically due to weak Cl···π interactions involving the 1,2-dithiole ring. This explains the thermotropic liquid crystal behavior of this compound.

4. CONCLUSIONS

A polymeric and anionic Cu(II) malonate complex with its corresponding protonated 2-amino-5-chloropyridine as counterion has been synthesized and the structure determined by single-crystal X-ray diffraction. A multitude of salt bridges are formed in this structure connecting the protonated 2-amino-5-chloropyridines and the malonate ligands of the polyanion. They participate in unprecedented sb···π and lp···π interactions that have been evaluated using theoretical calculations. One of the protonated 2-amino-5-chloropyridine moieties interacts with only one oxygen atom of the malonate ligand and a water molecule, freeing an oxygen atom to interact with the salt bridge. Because the formation of salt bridges is common in enzymes, both interactions, sb···π and lp···π interactions, might have potential importance in some biological systems. Furthermore, the three-centered Cl···Cl interaction observed in the crystal structure has been studied theoretically and compared with similar structures already reported in the literature.

■ ASSOCIATED CONTENT

Supporting Information

X-ray crystallographic data in CIF format for 1 (CCDC no. 933114), Tables S1–S4, Figure S1, and theoretical methods. This material is available free of charge via the Internet at <http://pubs.acs.org>.

■ AUTHOR INFORMATION

Corresponding Author

*E-mail: som_rc_ju@yahoo.co.in (S.R.C.); toni.frontera@uib.es (A.F.); smukhopadhyay@chemistry.jdvu.ac.in (S.M.).

Notes

The authors declare no competing financial interest.

■ ACKNOWLEDGMENTS

M.M. gratefully acknowledges the University Grants Commission (New Delhi) for a junior research fellowship. P.M. thanks the Council of Scientific and Industrial Research (New Delhi, India) for a Junior Research Fellowship (09/096 (0641) 2010-EMR-I). S.M. is grateful to the PURSE programme in the Department of Chemistry, Jadavpur University for partial financial support of this work. This work was supported by the DGICYT of Spain (projects CTQ2011-27512/BQU and CONSOLIDER INGENIO 2010 CSD2010-00065, FEDER funds) and the Direcció General de Recerca i Innovació del Govern Balear (project 23/2011, FEDER funds).

■ REFERENCES

- Wheeler, S. E. Understanding Substituent Effects in Noncovalent Interactions Involving Aromatic Rings. *Acc. Chem. Res.* **2012**, *46*, 1029–1038.
- Quiñonero, D.; Frontera, A.; Deyà, P. M. Interplay between Ion-π and Ar/π van der Waals Interactions. *Comput. Theor. Chem.* **2012**, *998*, S1–S6.
- Notash, B.; Safari, N.; Khavasi, H. R. Anion-Controlled Structural Motif in One-Dimensional Coordination Networks via Cooperative Weak Noncovalent Interactions. *CrystEngComm* **2012**, *14*, 6788–6796.
- Estarellas, C.; Bauzá, A.; Frontera, A.; Quiñonero, D.; Deyà, P. M. On the Directionality of Anion-π Interactions. *Phys. Chem. Chem. Phys.* **2011**, *13*, 5696–5702.
- Watt, M. M.; Collins, M. S.; Johnson, D. W. Ion-π Interactions in Ligand Design for Anions and Main Group Cations. *Acc. Chem. Res.* **2012**, *46*, 955–966.
- Riley, K. E.; Hobza, P. On the Importance and Origin of Aromatic Interactions in Chemistry and Biodisciplines. *Acc. Chem. Res.* **2012**, *46*, 927–936.
- Barceló-Olivé, M.; Estarellas, C.; Raso, A. G.; Terrón, A.; Frontera, A.; Quiñonero, D.; Molins, E.; Deyà, P. M. Lone Pair-π vs π-π Interactions in 5-Fluoro-1-Hexyluracil and 1-Hexyluracil: a Combined Crystallographic and Computational Study. *CrystEngComm* **2010**, *12*, 362–365.
- Wang, D. X.; Wang, M. X. Anion-π Interactions: Generality, Binding Strength, and Structure. *J. Am. Chem. Soc.* **2013**, *135*, 892–897.
- Ballester, P. Experimental Quantification of Anion-π Interactions in Solution Using Neutral Host–Guest Model Systems. *Acc. Chem. Res.* **2012**, *46*, 874–884.
- Mitra, M.; Manna, P.; Seth, S. K.; Das, A.; Meredith, J.; Helliwell, M.; Bauzá, A.; Choudhury, S. R.; Frontera, A.; Mukhopadhyay, S. Salt-Bridge-π (Sb-π) Interactions at Work: Associative Interactions of Sb-π, π-π and Anion-π in Cu(II)-Malonate-2-Aminopyridine-Hexafluoridophosphate Ternary System. *CrystEngComm* **2013**, *15*, 686–696.
- Gallivan, J. P.; Dougherty, D. A. A Computational Study of Cation-π Interactions vs. Salt Bridges in Aqueous Media: Implications for Protein Engineering. *J. Am. Chem. Soc.* **2000**, *122*, 870–874.
- Barril, X.; Alemán, C.; Orozco, M.; Luque, F. J. Salt-Bridge Interactions: Stability of the Ionic and Neutral Complexes in the Gas Phase, in Solution, and in Proteins. *Proteins: Struct., Funct., Genet.* **1998**, *32*, 67–79.
- Brown, B. M.; Milla, M. E.; Smith, T. L.; Sauer, R. T. Scanning Mutagenesis of Arc Repressor as a Functional Probe of Operator Recognition. *Nat. Struct. Biol.* **1994**, *1*, 164–168.
- Andersson, H. S.; Figueredo, S. M.; Haugaard-Kedström, L. M.; Bengtsson, E.; Daly, N. L.; Qu, X.; Craik, D. J.; Ouellette, A. J.; Rosengren, K. J. The α-Defensin Salt-Bridge Induces Backbone Stability to Facilitate Folding and Confer Proteolytic Resistance. *Amino Acids* **2012**, *43*, 1471–1483.

- (15) Marquese, S.; Baldwin, R. L. Helix Stabilization by Glu⁻–Lys⁺ Salt Bridges in Short Peptides of De Novo Design. *Proc. Natl. Acad. Sci. U.S.A.* **1987**, *84*, 8898–8902.
- (16) Dvornikovs, V.; Smithrud, D. B. Investigation of Synthetic Hosts That Model Cation- π Sites Found at Protein Binding Domains. *J. Org. Chem.* **2002**, *67*, 2160–2167.
- (17) Inoue, Y.; Sugio, S.; Andzelm, J.; Nakamura, N. A Density Functional Study of the Receptor-Ligand Interaction: Stabilization Energy in Ammonium Salt-Aromatic Interactions. *J. Phys. Chem. A* **1998**, *102*, 646–648.
- (18) Norrby, P. O.; Lilje fors, T. Strong Decrease of the Benzene-Ammonium Ion Interaction upon Complexation with a Carboxylate Anion. *J. Am. Chem. Soc.* **1999**, *121*, 2303–2306.
- (19) ZarRc, S. D.; Popovic, D. M.; Knapp, E. W. Metal Ligand Aromatic Cation- π Interactions in Metalloproteins: Ligands Coordinated to Metal Interact with Aromatic Residues. *Chem.—Eur. J.* **2000**, *6*, 3935–3942.
- (20) SAINT, version 6.36a; Bruker-AXS Inc.: Madison, WI, 2002.
- (21) SMART, version 5.625; SADABS, version 2.03a; Bruker AXS Inc.: Madison, WI, 2001.
- (22) Sheldrick, G. M. A Short History of SHELX. *Acta Crystallogr., Sect. A* **2008**, *64*, 112–122.
- (23) Manna, P.; Seth, S. K.; Das, A.; Hemming, J.; Prendergast, R.; Helliwell, M.; Choudhury, S. R.; Frontera, A.; Mukhopadhyay, S. Anion Induced Formation of Supramolecular Associations Involving Lone pair- π and Anion- π Interactions in Co(II) Malonate Complexes: Experimental Observations, Hirshfeld Surface Analyses and DFT Studies. *Inorg. Chem.* **2012**, *51*, 3557–3571.
- (24) Das, S.; Muthukumaragopal, G. P.; Pal, S. N.; Pal, S. A One-Dimensional Assembly of a Square-Planar Copper(II) Complex with Alternating Short and Long Cu…Cu Distances. Metal Ion Spin-Exchange Via π - π Interactions. *New J. Chem.* **2003**, *27*, 1102–1107.
- (25) (a) Das, A.; Dey, B.; Jana, A. D.; Hemming, J.; Helliwell, M.; Lee, H. M.; Hsiao, T.-H.; Suresh, E.; Colacio, E.; Choudhury, S. R.; Mukhopadhyay, S. Effect of Protonated Aminopyridines on the Structural Divergences of M(II)-Malonate Complexes (M = Cu, Ni, Co). *Polyhedron* **2010**, *29*, 1317–1325.
- (26) Choudhury, S. R.; Jana, A. D.; Chen, C. Y.; Dutta, A.; Colacio, E.; Lee, H. M.; Mostafa, G.; Mukhopadhyay, S. pH-Triggered Changes in the Supramolecular Self-Assembly of Cu(II) Malonate Complexes. *CrystEngComm* **2008**, *10*, 1358–1363.
- (27) Choudhury, S. R.; Gamez, P.; Robertazzi, A.; Chen, C.-Y.; Lee, H. M.; Mukhopadhyay, S. Experimental Observation of Supramolecular Carbonyl- π / π - π /carbonyl and Carbonyl- π / π - π -anion Assemblies Supported by Theoretical Studies. *Cryst. Growth Des.* **2008**, *8*, 3773–3784.
- (28) Choudhury, S. R.; Jana, A. D.; Colacio, E.; Lee, H. M.; Mostafa, G.; Mukhopadhyay, S. Crowned Tetrameric Spirocyclic Water Chain: An Unusual Building Block of a Supramolecular Metal–Organic Host. *Cryst. Growth Des.* **2007**, *7*, 212–214.
- (29) Bondi, A. van der Waals Volumes and Radii. *J. Phys. Chem.* **1964**, *68*, 441–451.
- (30) Egli, M.; Sarkhel, S. Lone Pair-Aromatic Interactions: To Stabilize or Not to Stabilize. *Acc. Chem. Res.* **2007**, *40*, 197–205.
- (31) Jordão, A. K.; Ferreira, V. F.; Cunha, A. C.; Wardell, J. L.; Wardell, S. M. S. V.; Tiekkink, E. R. T. The Differing Influence of Halides upon Supramolecular Aggregation Through C–X… π Interactions in the Crystal Structures of (5-Methyl-1-(4-X-Arylamino)-1H-1,2,3-Triazol-4-Yl)Methanol Derivatives, X = H, F and Cl. *CrystEngComm* **2012**, *14*, 6534–6539.
- (32) Bader, R. F. W. A Quantum Theory of Molecular Structure and its Applications. *Chem. Rev.* **1991**, *91*, 893–928.
- (33) Dey, B.; Choudhury, S. R.; Suresh, E.; Jana, A. D.; Mukhopadhyay, S. Supramolecular Assemblies Involving Anion- π and Lone Pair- π Interactions: Experimental Observation and Theoretical Analysis. *J. Mol. Struct.* **2009**, *921*, 268–273.
- (34) Quah, C. K.; Hemamalini, M.; Fun, H.-K. 2-Amino-4-Methylpyridinium 2-Hydroxy-3,S-Dinitrobenzoate. *Acta Crystallogr.* **2010**, *E66*, o1933–o1934.
- (35) Lorenc, J.; Bryndal, I.; Syska, W.; Wandas, M.; Marchewka, M.; Pietraszko, A.; Lis, T.; Maćzka, M.; Hermanowicz, K.; Hanuza, J. Order–Disorder Phase Transitions and Their Influence on the Structure and Vibrational Properties of New Hybrid Material: 2-Amino-4-Methyl-3-Nitropyridinium Trifluoroacetate. *Chem. Phys.* **2010**, *374*, 1–14.
- (36) Smith, G.; Bott, R. C.; Rae, A. D.; Willis, A. C. The Modulated Crystal Structure of the Molecular Adduct of 2,4,6-Trinitrobenzoic Acid with 2,6-Diaminopyridine. *Aust. J. Chem.* **2000**, *53*, 531–534.
- (37) Thanigaimani, K.; Farhadikoutenaei, A.; Khalib, N. C.; Arshad, S.; Razak, I. A. 2-Amino-5-Methylpyridinium Trifluoroacetate. *Acta Crystallogr.* **2012**, *E68*, o3319–o3320.
- (38) Moghimia, A.; Alizadehb, R.; Aragonic, M. C.; Lippolis, V.; Aghabozorg, H.; Norouzid, P.; Isaia, F.; Sheshmanie, S. Synthesis, Characterization and X-ray Crystal Structure of a Chromium(III) Complex Obtained from a Proton-Transfer Compound Containing 1,10-Phenanthroline-2,9-dicarboxylic Acid and 2,6-Pyridinediamine. *Z. Anorg. Allg. Chem.* **2005**, *631*, 1941–1946.
- (39) Hemamalini, M.; Fun, H.-K. 2-Amino-5-Bromopyridinium Trifluoroacetate. *Acta Crystallogr.* **2010**, *E66*, o775.
- (40) Hemamalini, M.; Fun, H.-K. 2-Amino-5-Chloropyridinium Trifluoroacetate. *Acta Crystallogr.* **2010**, *E66*, o783–o784.
- (41) Hemamalini, M.; Fun, H.-K. 2-Amino-5-Methylpyridinium 2-Hydroxy-3,S-Dinitrobenzoate. *Acta Crystallogr.* **2010**, *E66*, o1194–o1195.
- (42) Fur, Y. L.; Bagieu, B. M.; Masse, R.; Nicoud, J.-F.; Lévy, J.-P. Crystal Engineering of Noncentrosymmetric Structures Based on 2-Amino-5-nitropyridine and n-Chloroacetic Acid Assemblies. *Chem. Mater.* **1996**, *8*, 68–75.
- (43) Hosmane, R. S.; Lim, B. B.; Summers, M. F. Rearrangements in Heterocyclic Synthesis. 2. Novel Transformations of 2-Aminonicotinonitrile and Anthranilonitrile. *J. Org. Chem.* **1988**, *53*, 5309–5315.
- (44) Lu, Y.-X.; Zou, J.-W.; Wang, Y.-H.; Yu, Q.-S. Bifurcated Halogen Bonds: An Ab Initio Study of the Three-Center Interactions. *J. Mol. Struct.: THEOCHEM* **2006**, *767*, 139–142.
- (45) Seregin, I. V.; Ovchinnikov, I. V.; Makhova, N. N.; Lyubetsky, D. V.; Lysenko, K. A. An Unexpected Transformation of 3,4-Diacylfuroxans Into 3-Acyl-4-Acylaminofurazans in the Reaction with Nitriles. *Mendeleev Commun.* **2003**, *13*, 230–232.
- (46) Rakitin, O. A.; Rees, C. W.; Williams, D. J.; Torroba, T. Cyclopenta-1,2-dithioboles, Cyclopenta-1,2-thiazines, and Methylenoindenes from New Molecular Rearrangements. *J. Org. Chem.* **1996**, *61*, 9178–9185.